Sensors and Actuators B 235 (2016) 86–93

Contents lists available at ScienceDirect

Sensors and Actuators B: Chemical

journal homepage: www.elsevier.com/locate/snb

Controlled synthesis of flower-like In_2O_3 microrods and their highly improved selectivity toward ethanol

Feng Huang, Wei Yang, Fei He, Shantang Liu*

Key Lab for Green Chemical Process of Ministry of Education, School of Chemistry and Environmental Engineering, Wuhan Institute of Technology, Wuhan 430073, PR China

ARTICLE INFO

Article history:
Received 22 September 2015
Received in revised form 7 May 2016
Accepted 11 May 2016
Available online 12 May 2016

Keywords:
Flower-like In_2O_3 microrods
Synergistic effect
Sensing properties
Limit of detection
Interfering gases

ABSTRACT

In this study, well-defined, flower-like In_2O_3 microrods were successfully synthesized by a facile one-step hydrothermal method and subsequent calcination. Various techniques such as scanning electron microscopy (SEM), X-ray diffraction (XRD), transmission electron microscopy (TEM), and N_2 adsorption–desorption analyses were employed to clarify the feature of as-prepared product, including morphology, crystal structure and BET surface area. Appreciable control on the morphology of as-synthesized In_2O_3 samples was attained by altering the weight ratio of glucose and urea. The results show that the flower-like In_2O_3 microrods are formed in presence of glucose and urea, owing to the synergistic effect of the template role of glucose carbon spheres and Ostwald ripening under an alkaline environment. Moreover, the ethanol gas sensing properties of the flower-like In_2O_3 microrods were further investigated. Because of the structural merits including porosity and easily penetrable multiple rods, the sensor based on these flower-like In_2O_3 microrods exhibited superior sensitivity toward ethanol with a limit of detection lower to 1 ppm. In addition, improved selectivity to ethanol of this sensor is also demonstrated in other interfering gases, including formaldehyde, methanol, toluene, acetone, carbon oxides (CO) and Hydrogen (H_2). Also, the ethanol sensor displays a good repeatability. These results thereby demonstrate a potential application in a gas sensor for detecting ethanol vapor.

1. Introduction

Nowadays, environmental protection and human health are attracting increasing concern because of the release of harmful gases and other possible disasters, which focuses significant attention to gas detection [1,2]. Owing to their excellent features including simple operation, low cost, high sensitivity, fast response and recovery speed, and high stability, a number of typical semiconducting metal oxides, such as SnO_2 [3,4], ZnO [5,6], WO_3 [7], and TiO_2 [8], have aroused significant interest for fabrications of gas sensors to monitor toxic, noxious and flammable gases. In particular, indium oxide (In_2O_3), as an important n-type semiconductor with low specific resistance and high stability, has been extensively investigated as gas sensing materials for detection of H_2S [9], CH_3COCH_3 [10], CO [11], NO_2 [12], C_2H_5OH [13], HCHO [14], *etc.*

It is well known that the gas-sensing properties of materials are significantly depended on their physical properties, such as morphology, crystal structure, grain size, specific surface areas, and the quantities of oxygen adsorption [15]. For years, several methods such as chemical vapor deposition [16], electrospinning [17–19], the hydrothermal method [8,20–23], and spray pyrolysis [24] have been employed to obtain functional micro/nanomaterials with controlled physical feature. Among these methods, the hydrothermal method has been considered to be the most practical and widely applicable method because of its simplicity, universality and process controllability [25]. Up to now, some groups have explored a large variety of In_2O_3 materials with distinct morphologies using hydrothermal approach. For instance, Song et al. have developed porous In_2O_3 nanospheres using $InCl_3$, citric acid, and urea as precursors through a hydrothermal process [26]. Recently, Dong et al. have reported rosette-like In_2O_3 microspheres using a hydrothermal method starting from $InCl_3$, HCl, ethanediamine and glycerol [27]. Arunkumar et al. have synthesized mesoporous In_2O_3 nanocubes in a hydrothermal condition by optimizing the ratio of $InCl_3$ with reaction medium (water/PEG ratio), the reaction temperature, and time [28]. However, despite the considerable efforts have been made in the past decade, several research groups still feel that it is a great challenge to fabricate some functional

* Corresponding author.
E-mail address: stliu@wit.edu.cn (S. Liu).

http://dx.doi.org/10.1016/j.snb.2016.05.060
0925-4005/

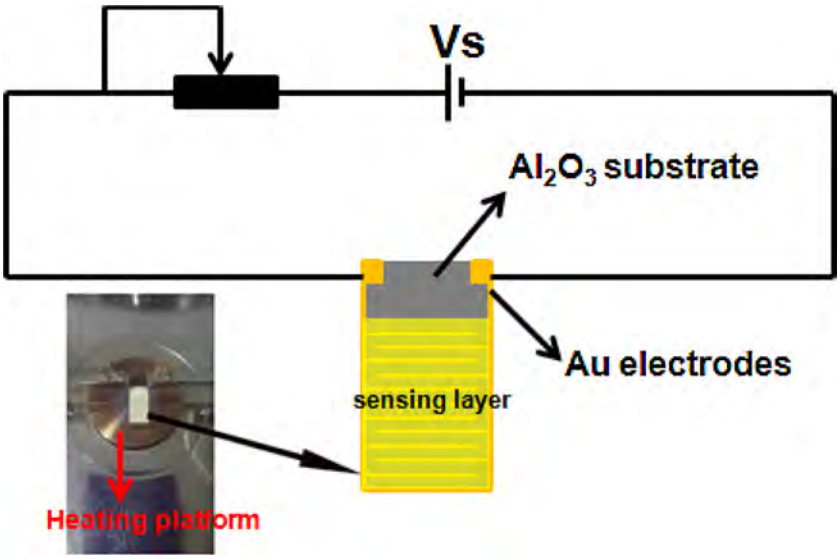

Scheme 1. Schematic of a typical gas sensor in a test circuit.

micro/nanomaterials with well-defined, unique, and certain morphologies.

Herein, we report novel flower-like In_2O_3 microrods using both glucose and urea as structure directing agents by a one-step hydrothermal method followed by calcination. To the best of our knowledge, such In_2O_3 microstructures have rarely been reported. Moreover, the formation of these flower-like structures can be controlled by altering the weight ratio of glucose and urea. In addition, a possible mechanism of this structure was also proposed in this case. To demonstrate its potential gas-sensing application, the flower-like In_2O_3 microrods-based sensor has been further prepared. The sensor exhibits a superior ethanol sensing performance with a limit of detection lower (LOD) to 1 ppm. At the same time, the sensor possesses an excellent selectivity toward ethanol, even though in other interfering gases (including formaldehyde, methanol, toluene, acetone, CO and H_2). Also, the ethanol sensor displays a good repeatability with standard deviations lower to 2%. Such results demonstrate the potential applications in detection of ethanol vapor.

2. Experimental

2.1. Synthesis of flower-like In_2O_3 microrods

All chemical reagents were analytical grade, and they were purchased from Sinopharm Chemical Reagent Co. Ltd., China without further purification. In a typical synthesis, 2 mmol of $InCl_3$ was first dissolved in 30 ml of deionized water, followed by the addition of 3.5 g of glucose and 3.5 g of urea under a vigorous stirring for 1 h. Afterwards, the mixed solution was transferred into a 50 ml Teflon-lined stainless-steel autoclave and maintained at 180 °C for 8 h. Subsequently, a black precipitate was obtained after the autoclave was allowed naturally to cool down to room temperature. The resulting precipitates were separated by centrifugation, followed washing with deionized water and ethanol for three times, alternately. After dried in a vacuum oven at 80 °C for 12 h, the flower-like In_2O_3 microrods were obtained by annealing the precipitates in a tube furnace at 500 °C for 2 h with a heating rate of 2 °C min^{-1} in air atmosphere. Likewise, the other products were prepared in the same manner, with the exception of the various weight ratios of glucose and urea (4:0, 4:1, 2:1, 1:2 and 0:4).

2.2. Characterization

The morphology and crystal structure of the products were examined by scanning electron microscopy (SEM, JEOL, and JSM-5510LV), transmission electron microscopy (TEM), and high-resolution electron microscopy (HRTEM, JEOL, JEM-2010). The crystalline phase in the samples was performed by an X-ray diffraction using Cu$K\alpha$1 radiation (λ = 0.15406 nm) at 40 kV and 20 mA. The diffraction patterns were recorded at a 2θ angle from 10° to 80° with a scanning rate of 5°/min.The BET surface areas were obtained from N_2 adsorption and desorption tests at 77 K using a NOVA2000e analyzer.

2.3. Fabrication and gas-sensing measurement

The as-synthesized products were ground and mixed with ethanol to form a homogenous paste (W/V = 10 mg/15 ml). Then, the paste was brushed onto an Al_2O_3 ceramic plate substrate (length, width and thickness were 10 mm, 20 mm, and 0.635 mm, respectively) to form a sensing channel between a pair of Au interdigitated electrodes (electrode and gap width were 0.18 mm and 0.18 mm, respectively), which had been previously printed on the substrate. Afterwards, the sensing layer on the substrate was dried at 80 °C for 2 h and subsequent annealing at 500 °C for another 3 h to improve the contact with Au electrodes. The thickness of sensing film was controlled by brushed number. The gas sensing properties of the sensors were measured by using a CGS-1TP intelligent test system (Beijing Elite Tech. Co., Ltd., China) under laboratory conditions (40% RH, 25 °C). Scheme 1 shows a typical sensor measured in a sensing platform. The measurement was conducted by a static process in a test chamber (18 l). The operation temperature of the sensor was conducted by a heating system. A typical testing procedure was as following: the as-fabricated sensor was placed into the chamber and then a given concentration of gas was injected into the chamber using a microsyringe. The concentration of the gas was controlled by the volume using a gas distribution method [29]. When the response reached a constant value, the test chamber was opened, and the sensor was allowed to recover in air. Since all test gases are reducing species, The sensor response was defined as $S = R_a/R_g$, where R_a and R_g represent the resistance of the sensor in air and the test gas, respectively. The response and recovery times

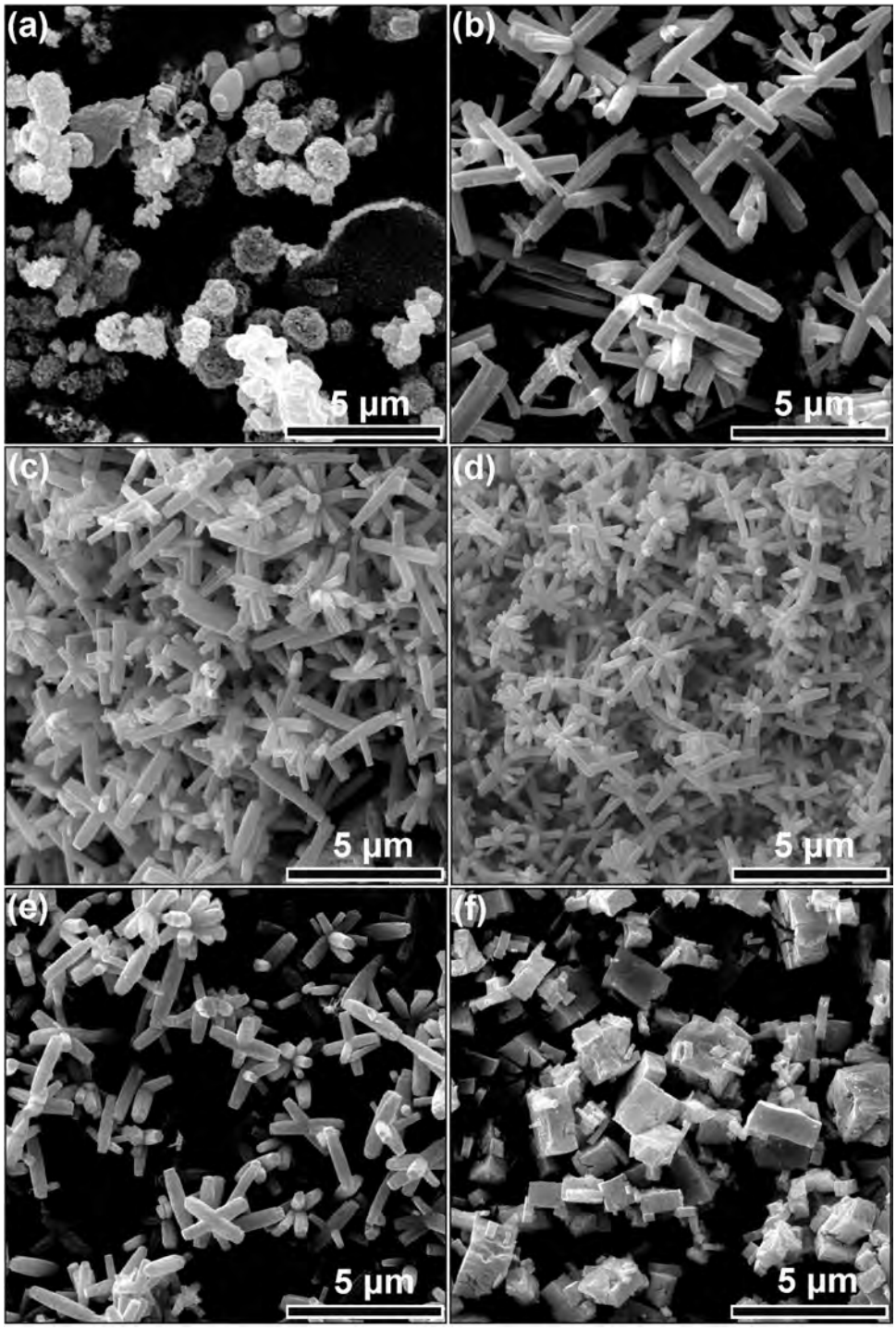

Fig. 1. SEM images of In_2O_3 samples prepared with different weight ratios of glucose and urea: (a) 4:0, (b) 4:1, (c) 2:1, (d)1:1, (e) 1:2, (f) 0:4.

were defined as the time taken by the sensor to achieve 90% of the total resistance change for adsorption and desorption processes.

3. Results and discussion

3.1. Morphology and structure

Fig. 1 shows typical SEM images of the obtained In_2O_3 samples. As observed in Fig. 1(a), the as-synthesized In_2O_3 exhibited an irregular microsphere structure in presence of glucose alone, whereas the microcubes with non-uniform shapes and size distribution were formed with the adding of urea alone (Fig. 1(f)). Interestingly, when both glucose and urea were used as additive reagents, the flower-like In_2O_3 microrods were obtained. As shown in Fig. 1(b)–(e), these In_2O_3 samples were self-assembled from microrods, and each individual microrod from the flower shared the same geometric center. The average diameters of these microrods were determined to be ~656 nm, 354 nm, 200 nm, and 514 nm for flower-like In_2O_3 microrods with different weight ratios of glucose and urea, respectively. Table 1 summarizes the according results about size characteristic of these In_2O_3 samples. For comparison, the In_2O_3 sample in Fig. 1(d) is selected for fabrication of a gas sen-

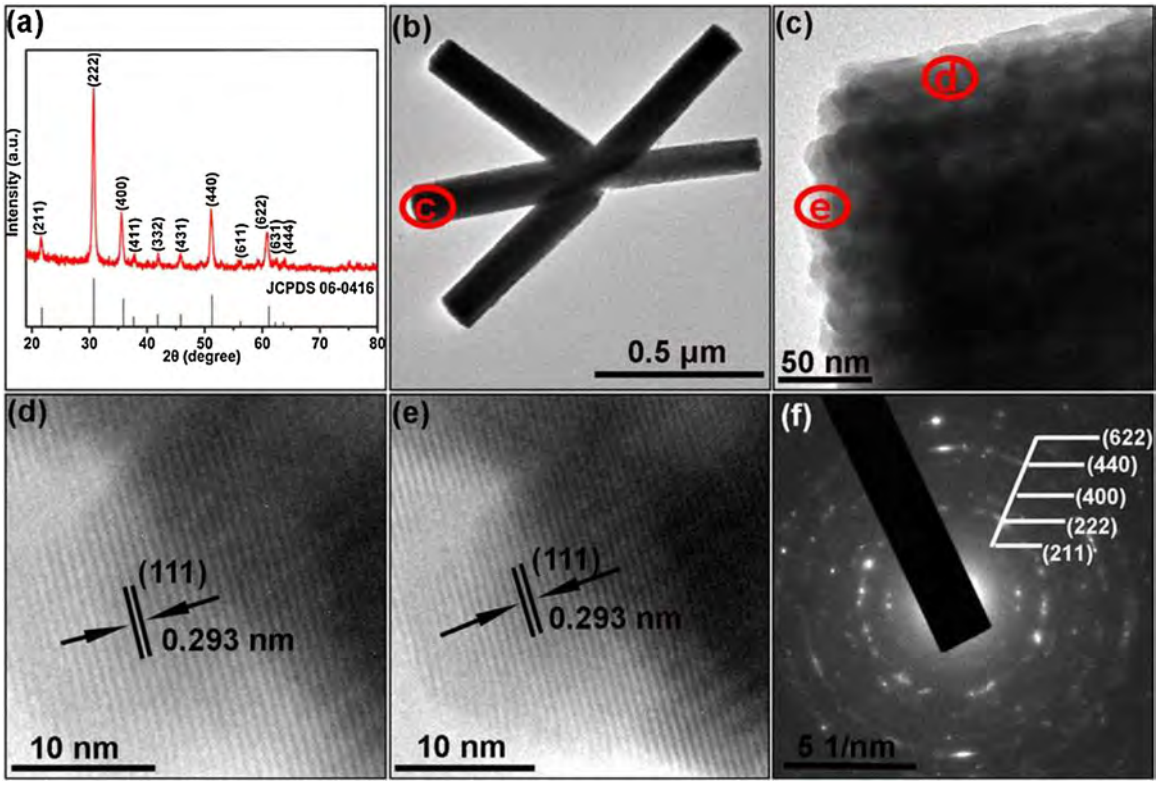

Fig. 2. (a) XRD patterns and (b) a typical TEM image of the flower-like In_2O_3 microrods; (c) an enlarged TEM image of the individual In_2O_3 microrod; (d and e) HRTEM image of the individual microrod at the different part; (f) SEAD pattern of the individual microrod.

Table 1
Different sizes of flower-like In_2O_3 microrods prepared by varying the weight ratios of glucose and urea.

M (glucose):M (urea)	4:1	2:1	1:1	1:2
Average length (μm)	2.05	1.11	0.67	0.86
Average diameter (nm)	656	354	200	514

sor because of its smallest diameter and shortest length, implying the highest surface-to-volume ratio (see Supporting information (SI), Fig. S1 and Table S1), which is favorable for gas adsorption.

To further investigate the crystal structure of the chosen In_2O_3 sample, it was also characterized by other techniques. As shown in Fig. 2(a), the crystal structure of the flower-like In_2O_3 microrods was examined by XRD technique. All the diffraction peaks were clearly assigned to the cubic structure of In_2O_3 (JCPDS No. 06-0461) [30]. Furthermore, impure peaks were not clearly observed in the XRD patterns, implying a high purity of the target sample. The crystal size of this sample was estimated by the Scherrer formula: $D = 0.89\lambda/\beta\cos\theta$, where D is the mean crystallite size, λ is the wavelength of the X-ray radiation (λ = 0.154 nm for Cu $K\alpha 1$ radiation), and β is the full-width at half-maximum of the diffraction peak at 2θ. As a result, the average crystallite size of the flower-like In_2O_3 microrods was approximately 16.8 nm. To obtain detailed information of morphology for flower-like In_2O_3 microrods, the TEM technique was employed. As shown in Fig. 2(b), the single flower-like In_2O_3 microrod was composed of multiple microrods with rough surfaces. It can be obviously seen in a higher resolution of TEM image (Fig. 2(c)) that these micro-shapes are composed of nanoparticles. The individual flower-like rods were also characterized by high-resolution TEM (HRTEM) in Fig. 2(e) and (f). The HRTEM image confirms that both the edge part and port part of In_2O_3 microrods exhibit clear lattice spacing values of 0.293 nm, corresponding to the (111) planes of In_2O_3 crystals. Meanwhile, the selected-area electron diffraction (SEAD) pattern in Fig. 2(f) demonstrates the structure of In_2O_3 microrods is polycrystalline structure in nature.

The porous characteristic of the flower-like In_2O_3 microrods was further analyzed by nitrogen physisorption isotherm techniques. As exhibited in Fig. 3, the as-obtained In_2O_3 products displayed a type IV isotherm with hysteresis loops in the range of 0.45–0.9 $P/P_{\bigcirc}$. The pore size distribution for the sample was calculated by the Barrett–Joyner–Halenda (BJH) model and desorption branch isotherm (inset of Fig. 3). A narrow pore size distribution peak was centered at approximately 7.4 nm, implying the formation of a mesopore structure (2–50 nm) in the sample [31]. In addition, the BET surface of the sample was estimated to be 25.15 m^2/g.

3.2. Growth mechanism

On the basis of all the above observations, a plausible growth mechanism for formation of the various In_2O_3 morphologies was schematically proposed in Fig. 4. For the In_2O_3 microspheres, their formation was conducted upon template effect of carbon spheres from glucose, and the detailed process was described as following. First, In^{3+} is produced after $InCl_3$ is dissolved in deionized water. A carbon sphere structure from glucose is obtained under hydrothermal conditions at 180 °C. Afterwards, In^{3+} can be easily adsorbed onto spheres because of a large amount of hydrophilic functional groups such as —OH and —C=O on their surface [32,33]. During this reaction process, the carbon spheres can act as the active sites for nucleation and crystallite growth of $In(OH)_3$ [34]. After calcinations, the carbon dioxide and water vapor are generated, resulting in the formation of In_2O_3 microsphere with a porous structure. For In_2O_3 microcubes, urea is added as precursor, and decompose and release OH^- ions under the hydrothermal conditions, which provide an alkaline environment; hence, In^{3+} will gradually be converted into $In(OH)_3$ crystal nucleus [35]. To

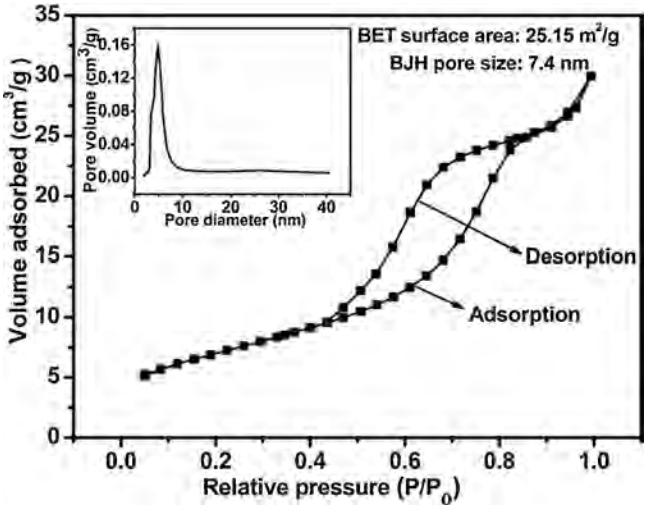

Fig. 3. Nitrogen gas adsorption–desorption isotherms and BJH pore size distribution (inset) of the flower-like In_2O_3 microrods.

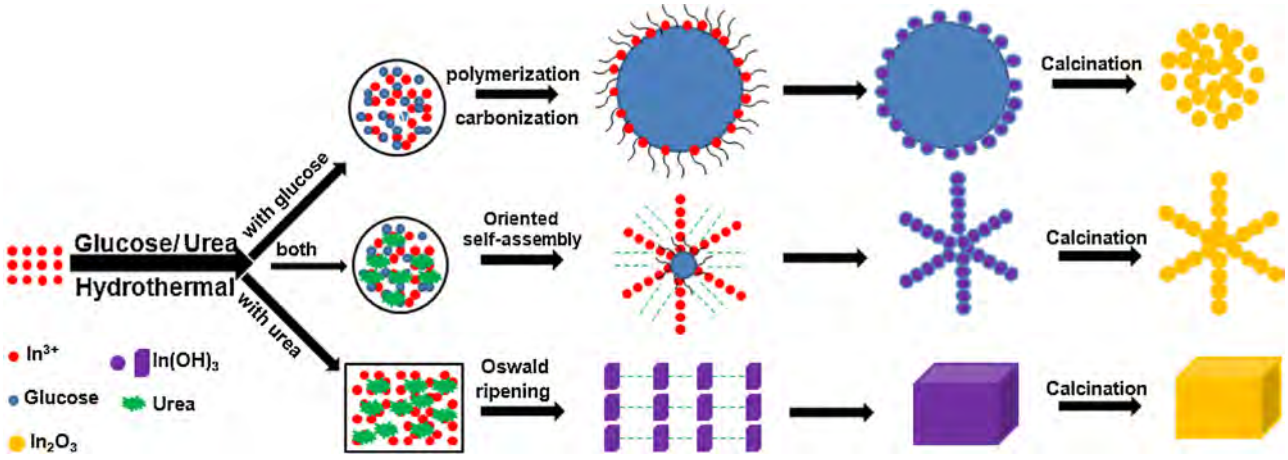

Fig. 4. Schematic of the growth mechanism for In_2O_3 with different morphologies.

decrease the surface area and free energy, the crystal nuclei of $In(OH)_3$ gradually grow into uniformly large cubes through Ostwald ripening process [36,37]. The In_2O_3 microcubes formed after the calcination of $In(OH)_3$ precursor. Interestingly, when both glucose and urea are added into the system, the products exhibited a flower-like microstructure, attributed to the synergistic effect of these two reagents. Glucose serves as a steric stabilizer, which is essential to form the whole framework. In the solution, the functional groups of carbon spheres can absorb In^{3+} ions, and then they are converted into $In(OH)_3$ when the urea is decomposed. Meanwhile, the increase in the $In(OH)_3$ seeds results in self-aggregation, and branches of microrods grow on the basis of a center in the presence of urea to reduce their surface energies through an oriented attachment self-assembly mechanism. As a result, a flower-like microstructure is formed. Furthermore, flower-like In_2O_3 microrods with different sizes can be controlled by altering the weight ratio of glucose and urea. The microrods become shorter and thinner with increased urea content, and their length and thickness increases when the weight ratio of urea to glucose exceeds 1:1. This phenomenon is probably explained by the competition of two reagents in directing structure formation. However, when the weight ratio reaches 1:1, the competition tends to balance.

3.3. Gas sensing properties of the flower-like In_2O_3 microrods

As we all know, In_2O_3 has been proved to be a widely used gas sensing material to detect different gases in daily life. Herein, in this study, a sensor based on the as-synthesized flower-like In_2O_3 microrods was used to investigate its ethanol sensing performance for the purpose of demonstrating an advantageous structure in gas-sensing application. For comparison, the other In_2O_3 morphologies were also fabricated for gas sensors in an identical manner. At first, the optimum working temperatures of these sensors were determined. Fig. 5(a) shows the sensor response to 100 ppm of ethanol at different operating temperatures, indicating the sensor response varied with different operating temperatures. The response significantly enhanced with an increased operating temperature from 200 °C to 300 °C, and then decreased with further increasing the operating temperature. And the response to 100 ppm ethanol reached its maximum at 300 °C. This phenomenon can be explained as following: generally, the optimum operating temperature can provide certain energy for activating the reaction between the target gas and adsorbed oxygen to ensure that the sensor exhibits the highest efficiency. However, it is not favorable for oxygen molecules to adsorb on the In_2O_3 surface at a relatively

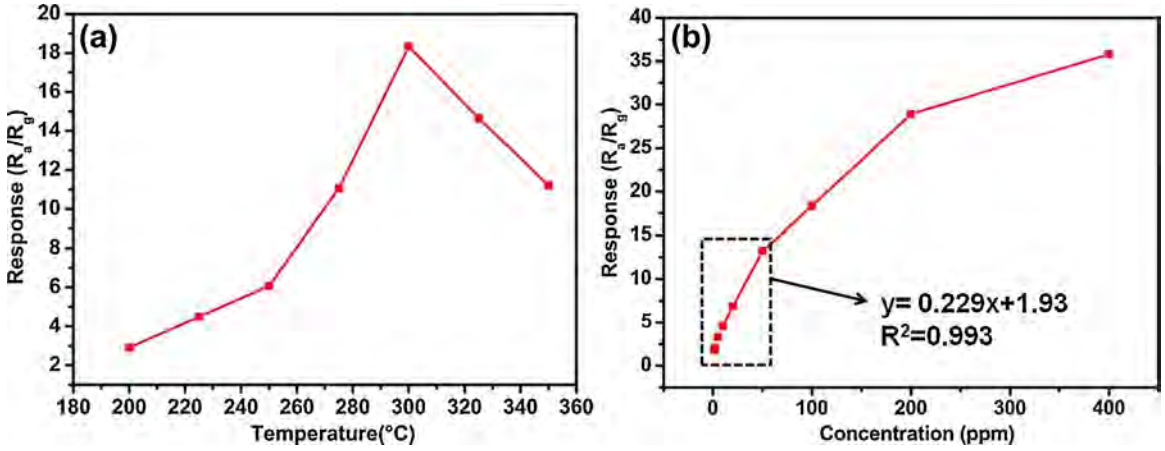

Fig. 5. (a) Sensor responses based on the flower-like In_2O_3 to 100 ppm of ethanol at different operating temperatures; (b) sensor responses to different concentrations (1–400 ppm) of ethanol at the optimum operating temperature of 300 °C.

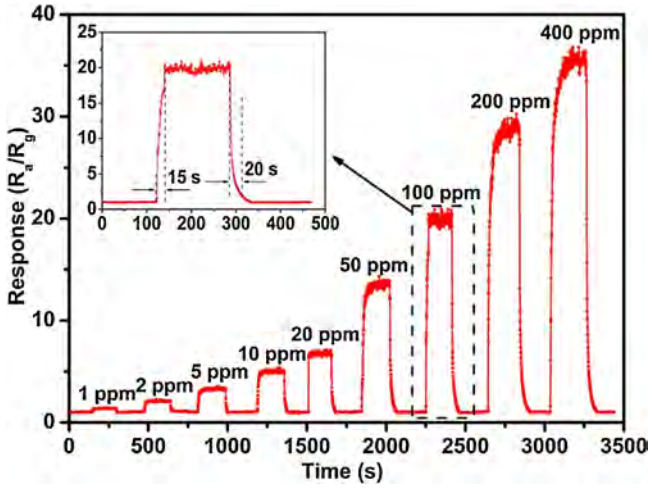

Fig. 6. Dynamic response curve of the flower-like In_2O_3 microrods-based sensor to ethanol with a concentration range from 1 ppm to 400 ppm (Inset: a typical response transient to 100 ppm of ethanol).

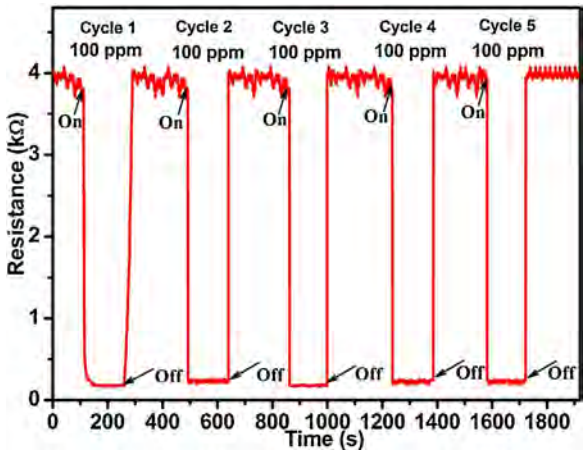

Fig. 7. Response and recovery curve of the flower-like In_2O_3 microrods-based sensor upon exposure of to 100 ppm of ethanol in quintuplicate cycles.

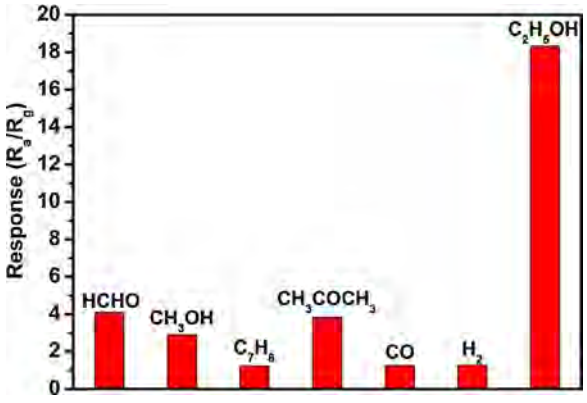

Fig. 8. Sensor responses of the flower-like In_2O_3 microrods to various gases with the same concentration (100 ppm) at 300 °C.

high temperature. Therefore, it is not suitable when the operating temperature is too low or too high, the balance between the chemical reaction and gas adsorption will form only at the optimum operating temperature [38]. Hence, 300 °C was chosen as the optimum operating temperature. Fig. 5(b) exhibits the sensor response to ethanol with different concentration ranging from 1 to 400 ppm. The response of sensor based on flower-like In_2O_3 microrods was significantly raised with increased ethanol concentration, and the limit of detection was lower to 1 ppm. Furthermore, a linear relationship of sensor response versus ethanol concentration ranging from 1 to 50 ppm was obtained ($y = 0.229x + 1.93$, $R^2 = 0.993$), implying that the ethanol vapor could be quantitative detected using this sensor. In addition, the sensor based on the flower-like In_2O_3 microrods showed a fast response and recovery speed toward ethanol with a concentration from 1 to 400 ppm, implying an amplitude response (Fig. 6). In addition, a typical transient response and recovery of the sensor to 100 ppm ethanol were only 15 s and 20 s, respectively (the inset of Fig. 6). To illustrate the structure advantages of the flower-like In_2O_3 microrods, the other In_2O_3 morphologies prepared in a batch but using different weight ratios of urea and glucose were fabricated into sensors using identical process, but showed relatively poor ethanol sensing (See SI, Fig. S2). Moreover, the repeatability of the flower-like In_2O_3 microrods-based sensor was investigated. As shown in Fig. 7, the sensor displays a good repeated response toward 100 ppm of ethanol with standard deviations lower to 2%.

Moreover, an excellent gas sensor must exhibit good selectivity to the target gas in the presence of other interfering gases, especially those with similar physicochemical properties [39]. Hence, a systematic test is examined to other types of gases, including formaldehyde (HCHO), methanol (CH_3OH), toluene (C_7H_8), acetone (CH_3COCH_3), carbon monoxide (CO), and hydrogen (H_2) at

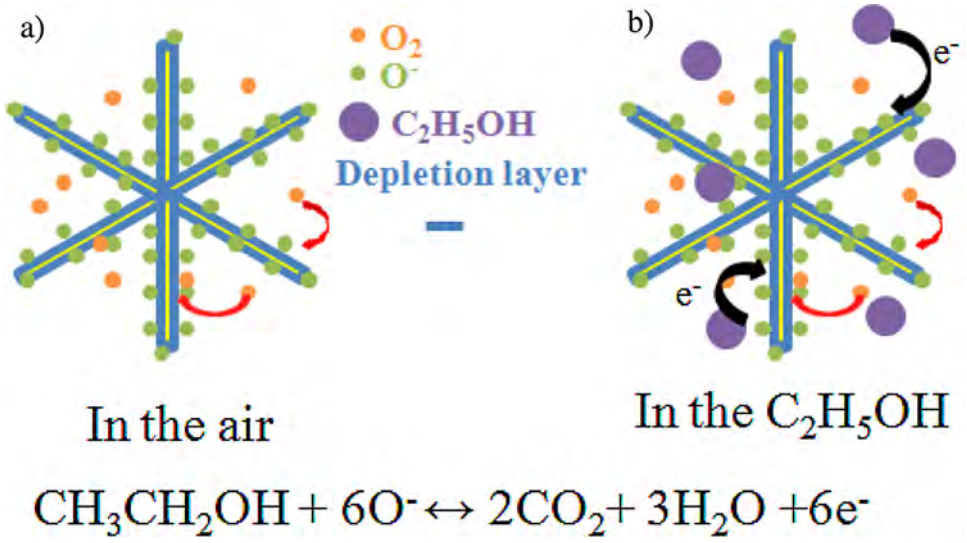

Fig. 9. Schematic illustration of the ethanol sensing process of the flower-like In_2O_3 microrods.

the same concentration (100 ppm). As shown in Fig. 8, the sensor highest response toward 100 ppm of ethanol (about 18.33), which is four times higher than those of formaldehyde, methanol, and acetone, and ten fold higher than those of C_7H_8, CO and H_2, respectively. From this viewpoint, flower-like In_2O_3 microrods displayed a highly improved selectivity toward ethanol. In comparison, other In_2O_3 morphologies-based sensors were also tested, however, they cannot display a selective sensing to ethanol (See SI, Fig.S3).

In this study, the ethanol sensing mechanism of the flower-like In_2O_3 microrods was discussed as well. The gas adsorption-desorption theory could be explained in our case. When the flower-like In_2O_3 microrods were exposed in the atmosphere, oxygen molecules can capture free electrons from the conduction band of In_2O_3 and form chemisorbed oxygen species (O^{2-}, O^-, O_2^-) adsorbed on In_2O_3 material surface (Fig. 9(a)). The resistance of the sensor increased because of the formation of depletion layers. When the In_2O_3 was exposed to ethanol, a reaction occurs between ethanol molecules and adsorbed oxygen species on the In_2O_3 surface (Fig. 9(b)). The captured electrons returned to the conduction band of In_2O_3, which lead to a remarkable decrease in sensor resistance. The whole process can be summarized as follows (Eqs. (1)–(4)):

$$O_2 + e^- \leftrightarrow O_2^- \quad (1)$$

$$O_2^- + e^- \leftrightarrow 2O^- \quad (2)$$

$$O^- + e^- \leftrightarrow O^{2-} \quad (3)$$

$$CH_3CH_2OH + 6O^- \leftrightarrow 2CO_2 + 3H_2O + 6e^- \quad (4)$$

In addition, the improved selective sensing to ethanol of flower-like In_2O_3 microrods may be attributed to the following aspects: firstly, the flower-like In_2O_3 microrods could provide more available active surface areas because of the unique microstructure and its own good physicochemical properties, thus enhancing the reaction between ethanol and the adsorbed oxygen at the optimum operating temperature of sensor [30]; secondly, among these gases, ethanol can attract the most electrons from adsorbed oxygen by Eqs. (4)–(10). Due to high adsorption of ethanol on the In_2O_3 surface and strong reactivity of ethanol with O^-, the sensor seemed to be more selective sensing to ethanol compared with methanol, formaldehyde and acetone. For C_7H_8, CO and H_2, they always exhibit poor reaction active with O^- on the In_2O_3 surface due to their high dissociation under this condition. As a result, the sensor exhibited naturally an enhanced selectivity toward ethanol against the other interfering gases in our study.

$$HCHO + 2O^- \leftrightarrow CO_2 + H_2O + 2e^- \quad (5)$$

$$CH_3OH + O^- \leftrightarrow HCHO + H_2O + e^- \quad (6)$$

$$C_7H_8 + 2O^- \leftrightarrow C_7H_6O + H_2O + 2e^- \quad (7)$$

$$CO + O^- \leftrightarrow CO_2 + e^- \quad (8)$$

$$H_2 + O^- \leftrightarrow H_2O + e^- \quad (9)$$

$$CH_3COCH_3 + O^- \leftrightarrow CH_3C^+O + CH_3O^- \quad (10)$$

4. Conclusions

In summary, a novel flower-like In_2O_3 microrods were successfully synthesized with glucose and urea as structure directing agents by a facile one-step hydrothermal method and subsequent calcination. In addition, the shaped and size of this unique microstructure can be well controlled by altering the weight ratio of glucose and urea. The gas sensing tests indicated that the flower-like In_2O_3 microrods-based sensor exhibited an excellent response toward ethanol with a limit of detection lower to 1 ppm. Meanwhile, this sensor displays a highly improved selectivity to ethanol against other interfering gases (including formaldehyde, methanol, toluene, acetone, CO and H_2). Furthermore, a good repeatability is also demonstrated for our sensor. Therefore, these results demonstrated a potential application for detections of ethanol using our sensor.

Acknowledgements

This work was financially supported by the National Natural Science Foundation of China (No.21471120), Natural Science Foundation of Hubei Province (2012IHA00201), Educational Commission of Hubei Province of China (T201306).

Appendix A. Supplementary data

Supplementary data associated with this article can be found, in the online version, at http://dx.doi.org/10.1016/j.snb.2016.05.060.

References

[1] W.F. Qin, L. Xu, J. Song, R.Q. Xing, H.W. Song, Highly enhanced gas sensing properties of porous SnO_2–CeO_2 composite nanofibers prepared by electrospinning, Sens. Actuators B 185 (2013) 231–237.

[2] L.L. Wang, Z. Lou, T. Fei, T. Zhang, Templating synthesis of ZnO hollow nanospheres loaded with Au nanoparticles and their enhanced gas sensing properties, J. Mater. Chem. 22 (2012) 4767–4771.

[3] R. Ab Kadir, Z.Y. Li, A.Z. Sadek, R. Abdul Rani, A.S. Zoolfakar, M.R. Field, J.Z. Ou, A.F. Chrimes, K. Kalantar-zadeh, Electrospun granular hollow SnO_2 nanofibers hydrogen gas sensors operating at low temperatures, J. Phys. Chem. C 118 (2014) 3129–3139.

[4] Z.J. Wang, Z.Y. Li, T.T. Jiang, X.R. Xu, C. Wang, Ultrasensitive hydrogen sensor based on Pd^0-loaded SnO_2 electrospun nanofibers at room temperature, ACS Appl. Mater. Interfaces 5 (2013) 2013–2021.

[5] L. Liu, S.C. Li, J. Zhuang, L.Y. Wang, J.B. Zhang, H.Y. Li, Z. Liu, Y. Han, X.X. Jiang, P. Zhang, Improved selective acetone sensing properties of Co-doped ZnO nanofibers by electrospinning, Sens. Actuators B 155 (2011) 782–788.

[6] M.M. Xu, Q. Li, Y. Ma, H.Q. Fan, Ni-doped ZnO nanorods gas sensor: enhanced gas-sensing properties, AC and DC electrical behaviors, Sens. Actuators B 199 (2014) 403–409.

[7] G.C. Xi, Y. Yan, Q. Ma, J.F. Li, H.F. Yang, X.J. Lu, C. Wang, Synthesis of multiple-shell WO_3 hollow spheres by a binary carbonaceous template route and their applications in visible-light photocatalysis, Chem. Eur. J. 18 (2012) 13949–13953.

[8] X.F. Wu, H.Y. Song, J.M. Yoon, Y.T. Yu, Y.F. Chen, Synthesis of core–shell Au@TiO_2 nanoparticles with truncated wedge-shaped morphology and their photocatalytic properties, Langmuir 25 (2009) 6438–6447.

[9] X.S. Liang, T.H. Kim, J.W. Yoon, C.H. Kwak, J.H. Lee, Ultrasensitive and ultraselective detection of H_2S using electrospun CuO-loaded In_2O_3 nanofiber sensors assisted by pulse heating, Sens. Actuator B 209 (2015) 934–942.

[10] S. Kim, S. Park, G.J. Sun, S.K. Hyun, K.K. Kim, C. Lee, Enhanced acetone gas sensing performance of the multiple-networked Fe_2O_3-functionalized In_2O_3 nanowire sensor, Curr. Appl. Phys. 15 (2015) 947–952.

[11] S.K. Lim, S.H. Hwang, D. Chang, S. Kim, Preparation of mesoporous In_2O_3 nanofibers by electrospinning and their application as a CO gas sensor, Sens. Actuators B 149 (2010) 28–33.

[12] X.L. Hu, L.Y. Tian, H.B. Sun, B. Wang, Y. Gao, P. Sun, F.M. Liu, G.Y. Lu, Highly enhanced NO_2 sensing performances of Cu-doped In_2O_3 hierarchical flowers, Sens. Actuators B 221 (2015) 297–304.

[13] S. Park, S. Kim, G.J. Sun, S. Choi, S. Lee, C. Lee, Ethanol sensing properties of networked In_2O_3 nanorods decorated with Cr_2O_3-nanoparticles, Ceram. Int. 41 (2015) 9823–9827.

[14] R.J. Hu, J. Wang, P.P. Chen, Y.W. Hao, C.L. Zhang, X.G. Li, Preparation of Cd-Loaded In_2O_3 hollow nanofibers by electrospinning and improvement of formaldehyde sensing performance, J. Nanomater. (2014) 1–7.

[15] C. Doroftei, P.D. Popa, F. Iacomi, Synthesis of nanocrystalline La–Pb–Fe–O perovskite and methanol-sensing characteristics, Sens. Actuators B 161 (2012) 977–981.

[16] J.B. Zhang, X.N. Li, S.L. Bai, R.X. Luo, A.F. Chen, Y. Lin, High-yield synthesis of SnO_2 nanobelts by water-assisted chemical vapor deposition for sensor applications, Mater. Res. Bull. 47 (2012) 3277–3282.

[17] Z. Li, Y. Fan, J. Zhan, In_2O_3 nanofibers and nanoribbons: preparation by electrospinning and their formaldehyde gas-sensing properties, Eur. J. Inorg. Chem. 2010 (2010) 3348–3353.

[18] C.H. Zhao, G.Z. Zhang, W.H. Han, J.C. Fu, Y.M. He, Z.X. Zhang, E.Q. Xie, Electrospun In_2O_3/α-Fe_2O_3 heterostructure nanotubes for highly sensitive gas sensor applications, CrystEngComm 15 (2013) 6491–6497.

[19] J.B. Mu, B. Chen, M.Y. Zhang, Z.C. Guo, P. Zhang, Z.Y. Zhang, Y.Y. Sun, C.L. Shao, Y.C. Liu, Enhancement of the visible-light photocatalytic activity of In_2O_3-TiO_2 nanofiber heteroarchitectures, ACS Appl. Mater. Interfaces 4 (2012) 424–430.

[20] H. Yu, S.M. Wang, C.H. Xiao, B.X. Xiao, P. Wang, Z.F. Li, M.Z. zhang, Enhanced acetone gas sensing properties by aurelia-like SnO_2 micro-nanostructures, CrystEngComm 17 (2015) 4316–4324.

[21] J.J. Zhao, M.B. Zheng, X.Y. Lai, H.J. Lu, N.W. Li, Z.X. Ling, J.M. Cao, Preparation of mesoporous In_2O_3 nanorods via a hydrothermal-annealing method and their gas sensing properties, Mater. Lett. 75 (2012) 126–129.

[22] X.M. Wang, C.Q. Yu, J.X. Wu, Y.D. Zhang, Template-free hydrothermal synthesis of ZnO microrods for gas sensor application, Ionics 19 (2012) 355–360.

[23] J.L. Tian, J. Wang, Y.W. Hao, H.Y. Du, X.G. Li, Toluene sensing properties of porous Pd-loaded flower-like SnO_2 microspheres, Sens. Actuators B 202 (2014) 795–802.

[24] P.P. Sahay, R.K. Nath, Al-doped ZnO thin films as methanol sensors, Sens. Actuators B 134 (2008) 654–659.

[25] W.D. Shi, S.Y. Song, H.J. Zhang, Hydrothermal synthetic strategies of inorganic semiconducting nanostructures, Chem. Soc. Rev. 42 (2013) 5714–5743.

[26] P. Song, D. Han, H.H. Zhang, J. Li, Z.X. Yang, Q. Wang, Hydrothermal synthesis of porous In_2O_3 nanospheres with superior ethanol sensing properties, Sens. Actuators B 196 (2014) 434–439.

[27] H.X. Dong, Y. Liu, G.H. Li, X.W. Wang, D. Xu, Z.H. Chen, T. Zhang, J. Wang, L. Zhang, Hierarchically rosette-like In_2O_3 microspheres for volatile organic compounds gas sensors, Sens. Actuators B 178 (2013) 302–309.

[28] A. Shanmugasundaram, B. Ramireddy, P. Basak, S.V. Manorama, S. Srinath, Hierarchical $In(OH)_3$ as a precursor to mesoporous In_2O_3 nanocubes: a facile synthesis route, mechanism of self-assembly, and enhanced sensing response toward hydrogen, J. Phys. Chem. C 118 (2014) 6909–6921.

[29] P. Sun, X. Zhou, C. Wang, X.M. Xu, G.Y. Lu, One-step synthesis and gas sensing properties of hierarchical Cd-doped SnO_2 nanostructures, Sens. Actuators B 190 (2014) 32–39.

[30] W. Zheng, X.F. Lu, W. Wang, Z.Y. Li, H.N. Zhang, Y. Wang, Z.J. Wang, C. Wang, A highly sensitive and fast-responding sensor based on electrospun In_2O_3 nanofibers, Sens. Actuators B 142 (2009) 61–65.

[31] W. Tang, J. Wang, P.J. Yao, X.G. Li, Hollow hierarchical SnO_2-ZnO composite nanofibers with heterostructure based on electrospinning method for detecting methanol, Sens. Actuators B 192 (2014) 543–549.

[32] X.W. Li, X. Zhou, H. Guo, C. Wang, J.Y. Liu, P. Sun, F.G. Liu, G.Y. Lu, Design of Au@ZnO yolk-shell nanospheres with enhanced gas sensing properties, ACS Appl. Mater. Interfaces 6 (2014) 18661–18667.

[33] J. Zhang, X.H. Liu, S.H. Wu, M.J. Xu, X.Z. Guo, S.R. Wang, Au nanoparticle-decorated porous SnO_2 hollow spheres: a new model for a chemical sensor, J. Mater. Chem. 20 (2010) 6453–6459.

[34] F. He, C. Zhang, D. Zhou, L. Cheng, T. Li, G.X. Li, Mesoporous core–shell TiO_2 walnuts for photocatalysts and photodetectors with improved performances, Dalton Trans. 43 (2014) 7599–7607.

[35] J. Qi, J. Chen, G.D. Li, S.X. Li, Y. Gao, Z.Y. Tang, Facile synthesis of core–shell Au@CeO_2 nanocomposites with remarkably enhanced catalytic activity for CO oxidation, Energy Environ. Sci. 5 (2012) 8937–8941.

[36] S.Q. Guo, X. Zhang, Z.W. Hao, G.D. Gao, G. Li, L. Liu, In_2O_3 cubes: synthesis, characterization and photocatalytic properties, RSC Adv. 4 (2014) 31353–31361.

[37] Q. Tang, W.J. Zhou, W. Zhang, S.M. Ou, K. Jiang, Size-controllable growth of single crystal $In(OH)_3$ and In_2O_3 nanocubes, Cryst. Growth Des. 5 (2005) 147–150.

[38] H. Shan, C.B. Liu, L. Liu, J.B. Zhang, H.Y. Li, Z. Liu, X.B. Zhang, X.Q. Bo, X. Chi, Excellent toluene sensing properties of SnO_2-Fe_2O_3 interconnected nanotubes, ACS Appl. Mater. Interfaces 5 (2013) 6376–6380.

[39] L. Xiao, S.M. Shu, S.T. Liu, A facile synthesis of Pd-doped SnO_2 hollow microcubes with enhanced sensing performance, Sens. Actuators B 221 (2015) 120–126.

Biographies

Feng Huang received his B.S. degree in Chemistry Engineering and Technology from Wuhan Institute of Technology in 2013. He is currently working towards the M.S. degree at Wuhan Institute of Technology under the supervision of Prof. Shantang Liu. His research interests focuses on the synthesis of metal oxides and their applications in gas sensors.

Wei Yang received his Ph.D. degree in analytical chemistry from Wuhan University at 2014. Currently, he is working as a lecturer in the School of Chemistry and Environmental Engineering, Wuhan Institute of Technology. His research focuses on the development of semiconductor gas sensors.

Fei He received the Ph.D. degree from Huazhong University of Science and Technology, China in 2014. Currently he is a lecturer of Wuhan Institute of Technology and focuses his research primarily on functional nanomaterials and environmental catalysis.

Shantang Liu received the Ph.D. degree from Perking University, China in 2000. He did his postdoctoral work at Weizmann Institute of Science, Israel from September 2000 to January 2004. After this, he worked as a postdoctoral researcher at Laval University, Canada from January 2004 to January 2006, and then as a postdoctoral researcher at Virginia Commonwealth University, USA from January 2006 to March 2007. Currently he is "Chutian Scholar Program" distinguished professors of Wuhan Institute of Technology and focuses his research primarily on sensitive materials, semiconductor sensors and nanocatalysts.